EFDA–JET–PR(10)53

Y. Lin, P. Mantica, T. Hellsten, V. Kiptily, E. Lerche, M.F.F. Nave, J.E. Rice,
D. Van Eester, P. C. de Vries, R. Felton, C. Giroud, T. Tala
and JET EFDA contributors

ICRF Mode Conversion Flow Drive in D(^{3}He) Plasmas on JET

ICRF Mode Conversion Flow Drive in D(^{3}He) Plasmas on JET

Y. Lin[1], P. Mantica[2], T. Hellsten[3], V. Kiptily[4], E. Lerche[5], M.F.F. Nave[6], J.E. Rice[1], D. Van Eester[5], P. C. de Vries[7], R. Felton[4], C. Giroud[4], T. Tala[8] and JET EFDA contributors*

JET-EFDA, Culham Science Centre, OX14 3DB, Abingdon, UK

[1]MIT Plasma Science and Fusion Center, Cambridge, MA 02139, USA
[2]Istituto di Fisica del Plasma CNR-EURATOM, via Cozzi 53, 20125 Milano, Italy
[3]Association EURATOM-VR, Fusion Plasma Physics, EES, KTH, Stockholm, Sweden
[4]EURATOM/CCFE Fusion Association, Culham Science Centre, Abingdon, OX14 3DB, UK
[5]LPP-ERM/KMS, Association Euratom-Belgian State, TEC, B-1000 Brussels, Belgium
[6]Associação EURATOM/IST, Instituto de Plasmas e Fusão Nuclear, 1049-001 Lisbon, Portugal
[7]FOM Institute Rijnhuizen, Association EURATOM-FOM, Nieuwegein, the Netherlands
[8]Association EURATOM-Tekes, VTT, P. O. Box 1000, FIN-02044 VTT, Finland
** See annex of F. Romanelli et al, "Overview of JET Results", (23rd IAEA Fusion Energy Conference, Daejon, Republic of Korea (2010)).*

Preprint of Paper to be submitted for publication in
Plasma Physics and Controlled Fusion

ABSTRACT

ICRF mode conversion has been shown to drive toroidal flow in JET D(^{3}He) L-mode plasmas: $B_{t0}=3.45$T, $n_{e0} \sim 3\times10^{19}$ m^{-3}, $I_p = 2.8$ and 1.8MA, $P_{RF} \le 3$MW @ 33MHz and -90^o phase. Central toroidal rotation in the counter-I_p direction, with $\omega_{\phi 0}$ up to 10krad/s ($V_{\phi 0} \sim 30$km/s, central thermal Mach number $M_{th}(0) \sim 0.07$, and Alfven Mach number $M_A(0) \sim 0.003$) has been observed. The flow drive effect is sensitive to the ^{3}He concentration and the largest rotation is observed in the range of $n_{He3}/n_e \sim 10\%$-17%. The rotation profile is peaked near the magnetic axis, and the central rotation scales with the input RF power. The effective torque density profile from the RF power has been calculated and the total torque is estimated to be as high as 50% of the same power from neutral beam injection, and a factor of 5 larger than the direct momentum injection from the RF waves. RF physics modeling using the TORIC code shows that the interaction between the mode converted ion cyclotron wave and the 3He ions, and associated asymmetry in space and momentum may be key for flow drive.

1. INTRODUCTION

Plasma rotation has been shown to be beneficial for tokamak plasma performance. Experimentally, sheared flow has been shown to improve plasma confinement [1, 2, 3], and a large toroidal rotation can help stabilize MHD modes [4,5], but the issue of plasma rotation drive and control on ITER is far from being resolved. Recently, significant flow drive has been observed on Alcator C-Mod using Ion Cyclotron Range of Frequency (ICRF) waves via mode conversion in L-mode D(^{3}He) plasmas [6,7]. The result from Alcator C-Mod suggests that ICRF mode conversion is a potential flow drive method for ITER and future fusion devices. This paper reports the results from a collaborative study by the Alcator C-Mod and JET teams in investigating mode conversion flow drive on JET.

In multi-species tokamak plasmas, the application of ICRF waves typically involves two scenarios - Minority Heating (MH) and Mode Conversion (MC) - depending on the relative concentration of species. In the minority heating regime, for instance, in plasmas with D majority and a small fraction of externally puffed ^{3}He minority, fast magnetosonic waves (fast wave, or FW) launched from the antenna are first absorbed by the ^{3}He ions at the ^{3}He cyclotron resonance layer. This minority heating scheme requires a low minority concentration, and for D(^{3}He) plasmas, the ^{3}He concentration $X[^3He] \equiv n_{He3}/n_e$, needs to be no more than a few percent so that the D-^{3}He hybrid layer is sufficiently close to the ^{3}He cyclotron resonance [8]. The fast wave and ^{3}He ion interaction benefits from the left-handed wave polarization at the D-^{3}He hybrid layer. The high energy ^{3}He tail generated by this mechanism slows down via pitch angle scattering and collisional friction, and results in heating both bulk ions and electrons. As long as the hybrid layer is within the Doppler broadened cyclotron resonance, most RF power will be absorbed through the minority heating mechanism. In contrast, in the Mode Conversion (MC) heating regime, a large $X[^3He]$ moves the D-^{3}He hybrid layer farther away from the ^{3}He resonance towards the high field side. Because of the large separation between the hybrid layer and cyclotron resonance, the fast waves only weakly interact with the ^{3}He ions at the cyclotron resonance, and they are converted to other waves near the D-^{3}He hybrid layer

(also called the mode conversion layer). The transition from minority heating to mode conversion is gradual vs. X[^{3}He], and the physics of mode converted waves and their interaction with ions and electrons is complicated. The two MC wave branches - the Ion Bernstein Waves (MC IBW) and Ion Cyclotron Waves (MC ICW) – were previously studied theoretically [9, 10] and experimentally measured on Alcator C-Mod [11, 12]. They have also been further studied in numerical simulations [13]. Mode conversion electron heating in D(^{3}He) plasmas has been studied in detail on JET [14, 15], and it has also been used routinely for direct electron heating for electron transport studies [16]. Inverted mode conversion scenarios have also been studied on JET [17]. Besides being used for electron heating, mode conversion has also been used for sawtooth control [18]. Mode conversion flow drive with the ^{3}He concentration in the intermediate range between minority heating and pure MC electron heating has been demonstrated on Alcator C-Mod [6, 7], but the physical mechanism behind the phenomenon is not yet fully understood.

The study of plasma rotation in tokamaks is currently a very active research field [e.g.,19, 20, 21, 22, 23, 24]. Plasma rotation falls into two general categories: intrinsic and externally driven. Intrinsic rotation exists independent of the external momentum input or auxiliary heating methods, and it has been observed on many tokamaks [19, 20, 21, 25, 26]. For ITER and future reactors, an actuator for active intrinsic rotation control will be limited due to its correlation to plasma pressure and lack of rotation profile control. In present tokamaks, externally driven rotation is mainly from neutral beam injection as a by-product of beam heating with direct angular momentum input to the plasma. The NBI driven rotation on JET has reached $\omega_{\phi 0} \sim 220$krad/s [27]. However, for ITER, the neutral beam energy will be significantly higher in order to penetrate the expected higher density plasma and larger machine size, and this requirement will result in a much lower torque per MW beam power. Moreover, even with large amounts of NBI power, the fraction of beam particles in ITER will be much smaller than in the typical JET experiments. Beam driven rotation is thus presumed to be small in ITER.

Many efforts have been made on present tokamaks in search of an efficient RF flow drive method that may also be applicable on ITER and beyond. Externally launched ICRF waves have been studied in a number of experiments without great success in flow drive. Experimentally, ICRF minority heated plasmas show no evidence of direct RF driven rotation. The rotation in ICRF minority heated plasmas on Alcator C-Mod has the same trend versus plasma stored energy as the rotation in Ohmic plasmas [28,29]. Results from JET [30], Tore-Supra [31,32] and ASDEX-Upgrade [33] all show that the contribution of ICRF minority heating to rotation is intrinsic, i.e., not directly from the RF power absorption but rather indirectly due to the change in plasma temperature or plasma pressure. On JET, the rotation in L-mode plasmas (Ohmic or with ICRF) is typically small. The central toroidal angular velocity $\omega_{\phi 0} \leq 10$krad/s, and it is insensitive to the input RF power. The rotation is usually in the same direction as the plasma current (co-I_p) at high Ip and in the counter-I_p direction at low I_p [34,35]. Direct wave momentum in minority heating has been shown to directly drive toroidal rotation on JET [36]. The inferred rotation change $\Delta\omega_{\phi 0}$ from experimental measurement is less than 0.5krad/s per MW input of the directional fast waves, thus this method is not sufficient

to have significant effects on JET plasmas given the total available ICRF power. Studies on Alcator C-Mod have found a promising efficient flow drive method via ICRF mode conversion [6, 7], and further studies on plasma and RF parametric dependences have been carried out [37, 38]. JET is approximately a factor of 100 larger than Alcator C-Mod in terms of plasma volume, and the wave frequencies, magnetic field and current density are all different. In this paper, we report on a flow drive effect in JET experiments with ICRF mode conversion.

The paper is organized as follows. In Section 2, the experimental setup is described. In Section 3, the parametric dependence of the toroidal rotation is presented. In Section 4, we estimate the effective torque via RF power modulation. In Section 5 we show the fast ion characteristics from experimental measurement. The RF power deposition profile is analyzed from experimental data and numerical simulation in Section 6. In Section 7, we propose a hypothesis on the flow drive mechanism based on the mode conversion process, followed by discussion in Section 8 and summary in Section 9.

2. SETUP OF THE MODE CONVERSION FLOW DRIVE EXPERIMENT

The experiment was carried out in JET L-mode plasmas: $B_{t0} = 3.45$T, $I_p = 2.8$MA and 1.8MA, central density $n_{e0} \sim 3\times10^{19}$ m^{-3} during flat top. A total of 13 plasma pulses were obtained in this experiment. The plasma current was clockwise as seen from the top of the tokamak, and in the same direction as the toroidal B field. All the plasmas were in D majority with external ^{3}He puffing, and the concentration X[^{3}He] was feedback controlled in real-time using the method described in Refs. [14] and [15]. The ^{3}He concentrations referred to in this paper are estimated from visible spectroscopy light in the divertor, linking relative light intensities to relative concentrations, relying on an expression routinely adopted to control the ^{3}He injection in real time during the experiments. The cross section for a typical pulse in this experiment is shown in Figure 1.

All the ICRF power was launched via the A2 antennas on JET at 33MHz [39,40]. At $B_{t0} = 3.45$T, the ^{3}He ion cyclotron resonance layer was about 20 cm to the Low Field Side (LFS) of the magnetic axis. For X[^{3}He] ~ 13%, the D -^{3}He hybrid layer was about 10cm to the high-field-side of the magnetic axis. All the plasmas had a lower single null shape and were in L-mode confinement. The ICRF antennas were operated at -90^o phasing, i.e., the launched fast waves were toroidally asymmetric and predominantly in the counter-I_p direction.

In Figure 2, we show the data traces of JET Pulse No: 78845 from this experiment. In this plasma, we have $I_p = 2.8$MA, $P_{RF} = 2.5$MW, and later the RF power is also modulated to help us determine the flow drive torque and RF power deposition profile. X[^{3}He] is under feedback control (Fig. 2-(c)), and for this plasma, it is mostly at the level between 10% and 14%. To study the rotation that is different than the intrinsic rotation in ICRF minority heating, we vary the ^{3}He level pulse by pulse and monitor the change in toroidal rotation. Neutral beam blips are injected every second for rotation profile measurement (Fig. 2(d)). Shown in Fig. 2(e) is the toroidal rotation ω_ϕ of C^{6+} impurity ions, deduced from the Doppler shift of the active charge exchange spectrum measured by the core Charge Exchange Recombination Spectroscopy (CXRS) system [41, 42]. In this pulse, central rotation is in the counter-I_p direction ($\omega_{\phi 0} < 0$) for all the neutral beam blips for $t < 11$sec. Only at $t > 11$sec with

a continuous neutral beam injection and modulated ICRF power, the central rotation changes to the co-Ip direction. Electron density, temperature and B_{t0} traces are shown in Fig. 2(f), (g) and (i).

In the experiment, B_t and I_p are co-directional, and injecting ~1MW beam blips for the rotation measurement introduces a co-I_p angular momentum. As a result, the magnitude of the counter-I_p rotation measured during a beam blip tends to become smaller in time, and sometimes the rotation becomes co-I_p. To minimize this systematic bias introduced by the beam injection, we only use the average of the first 3CXRS data points within 30ms after the beam turn-on. As discussed in Refs. [34, 35], this treatment can minimize the co-I_p bias to less than 2krad/s and the resulting rotation profile can realistically reflect the plasma rotation just prior to the beam injection. The CXRS data from the beam blips prior to the RF power are also discarded because the CXRS signals are too weak due to low carbon density levels. The data from the inner-most channel at R = 2.88m, albeit also showing large counter-I_p rotation, are not used because of the concern of large error associated with this channel. These JET L-mode plasmas do not have large bulk plasma pressure gradients, therefore the difference in the bulk plasma rotation and the C^{6+} rotation is presumed small [35]. Parametric dependence of the rotation is studied in Section 3, and torque density is estimated in Section 4.

In Fig. 2(h), we show the photo-multiplier signal from the Scintillator Probe (SP) diagnostic [43,44], located just below the mid-plane of the torus. The SP provides the information on the pitch angle and gyro-radius of the ions that hit the scintillator plate after passing a collimator. In the plasmas of this experiment, the main contribution to the SP signal comes from the 3.6MeV α-particles, born from the nuclear reaction between D and ^{3}He. The existence of these fast α-particles indicates a hot ^{3}He ion population (and the signal is also enhanced by the injected D-beam). γ-ray spectroscopy data are also used to study the behavior of the hot ions [45]. Characteristics of the fast ions in this experiment are discussed in Section 5.

3. ROTATION PROFILE AND ITS DEPENDENCE ON X[^{3}HE], I_P, P_{RF}, AND W_{DIA}

The rotation profile is found to be very sensitive to the ^{3}He concentration. In Figure 3, we compare the rotation profiles from I_p = 2.8MA pulses at t ~ 7sec (after I_p reaches flattop). At X[^{3}He] < 0.5% (Pulse No: 78825) and X[^{3}He] ~ 4% (Pulse No: 78826), the rotation profiles are nearly flat and in the co-I_p direction, ω_ϕ ~ 1-4 krad/s, similar to the profiles previously reported in ICRF minority heated plasmas that have high I_p and near-axis heating [34, 35]. When the X[^{3}He] level is higher, X[^{3}He] ~ 10%-17%, centrally peaked counter-I_p rotation profiles are observed. Under this condition, the rotation is peaked for r/a < 0.4, but for the outer half of the plasma, it is close to zero but still in the co-Ip direction. A maximum central rotation $\omega_{\phi 0}$ ~ 10krad/s (~30km/s) has been observed in this experiment, which corresponds to central thermal Mach number $M_{th}(0) \sim 0.07$, and Alfven Mach number $M_A(0) \sim 0.003$. At even higher ^{3}He levels, X[^{3}He] ~ 25% (Pulse No: 78840), the counter-I_p rotation is again smaller.

The ^{3}He dependence can also be clearly seen in Figure 4, where only rotations at R = 3.04m and R = 3.69m are plotted versus X[^{3}He]. Again, it shows strong central counter-I_p rotation at X[^{3}He] ~

10%-17%, and also reduced edge rotation. While at the low X[3He] levels, the nearly flat profiles are similar to previously observed slow co-I_p rotation.

In our experiment, all but one of the plasma pulses were at 2.8MA. Interestingly, in this 1.8MA Pulse No: (78848), we observed larger counter-Ip rotation than the corresponding 2.8MA plasma Pulse No: (78845) at similar X[^{3}He] ≈ 12%-13%, PRF and plasma density (Figure 5). In a previous study [34], it was found that low current plasmas, both Ohmic and ICRF minority heated, have a higher tendency to show hollow rotation profiles. A hollow profile was observed in H minority heating with the resonance in the high field side of the magnetic axis (Pulse No: 66310). But the study also found that when the resonance is on the LFS, the rotation profile tends to be flat at this low current, which is opposite to the present observation.

In Figure 6, we plot the rotation from all the beam blips of the plasma pulses in this experiment versus the RF power level, including 2.8MA and 1.8MA. At R = 3.04m, a linear trend of rotation versus PRF exists for X[^{3}He] ~ 6%-18%, i.e., larger counter-I_p rotation at higher RF power. Note the data points from the 1.8MA pulse also lie closely with the 2.8MA pulses. The dependence of RF power indicates that the RF power (or RF momentum) is directly involved in the flow drive process. The approximately linear RF power dependence is similar to the result from Alcator C-Mod. This observation, at $\Delta\omega_{\phi 0}$ ~ 2 krad/s per MW ICRF power, is about a factor of 4 larger than the observed rotation difference in a previous study due to momentum input from the directional fast waves in the D(^{3}He) minority heating scenario [36]. For X[^{3}He] < 5%, there is little or no dependence on PRF and all the rotation is about 2krad/s in the co-I_p direction. The weak (or zero) PRF dependence in the minority heating regime is consistent to previous JET result in ICRF minority heated plasmas [34]. There are not enough data points from X[3He] ~ 22%-26% to conclude a clear power dependence. In contrast, at R = 3.69m, the co-I_p rotation is smaller and closer to zero for X[^{3}He] in the intermediate range, and seems independent of the RF power applied for all X[^{3}He] values in the MC regime.

In Figure 7, we compare the rotation in the center (R = 3.04m) and edge (R = 3.69m) versus plasma stored energy W_{dia}. For 6% < X[^{3}He] < 18%, there is a weak trend versus W_{dia}, but it is much more scattered than the one shown in Figure 6-(a). Also the data points from the 1.8MA pulse are significantly separated from those of the 2.8MA pulses, indicating that W_{dia} could be a less important parameter than PRF that affects the observed rotation. For edge rotation, as show in Figure 7(b), no dependence is seen versus W_{dia}, unlike the correlation established for rotation in the minority heating regime in Ref. [34]. All the pulses have the same density, thus no density dependence can be inferred.

The results shown in Figure 3 to Figure 7 suggest that for the intermediate X[^{3}He], a mechanism has introduced a counter-I_p torque near the center of the plasma. Resulting from this torque, the central rotation seems to scale with the RF power, while the rotation in the outer-half is also affected although the effect is weaker. The torque density will be estimated in the next section.

4. TORQUE DENSITY PROFILE AND TOTAL TORQUE FROM THE ICRF POWER

Because the momentum input from the neutral beam is in the co-I_p direction, the observed counter-I_p rotation during ICRF can be confidently ruled out as an artificial effect caused by the beam momentum. The beam torque would actually cause an underestimate of the counter-I_p RF driven flow. In Figure 8(a), we show the evolution of the rotation traces at different major radii in Pulse No: 78847 (X[^{3}He] ~ 13%) with continuous 1.2MW beam power and modulated RF power. In order to show the trend more clearly, the rotation traces from CXRS in Figure 8(a) have been smoothed by 50ms. RF power of 1.8MW is applied at t = 11.35sec, 0.8sec after the start of the beam and after the beam-driven co-Ip rotation profile has become steady. The turn-on of the ICRF power introduces a decrease of the magnitude of the co-I_p rotation near the plasma center ($R \leq 3.35$m). When the RF power is shut off, the rotation in this region increases being driven by the continuous beam. At the outer half of the plasma ($R \geq 3.41$m), the effect from the RF is smaller. The first RF turn-on introduces the largest rotation decrease, and the following RF turn-ons do not have the same large effect. This is because the momentum confinement time in this plasma is longer than the RF modulation period and the rotation has been approaching a new equilibrium at lower magnitude after adding the RF power.

Figure 8(b) and (c) show T_i and T_e traces respectively. The T_e signals are from a 96-channel ECE system [46], and the T_i signals are from the CXRS system. Like the rotation traces, the T_i traces shown in the figure have also been smoothed by 50ms. Sawtooth oscillations seen in both signals have irregular periods and are not locked by the RF modulation. At RF power transitions, instantaneous breaks-in-slope are clearly evident in the core T_e signals, suggesting direct RF power deposition on electrons. Because of the poor temporal resolution of T_i signals, the breaks-in-slope in the T_i signals are not meaningful, but a coarse power deposition profile can still be obtained from Fourier analysis of the RF power modulation. Detailed RF power deposition profiles to electrons and ions will be discussed in Section 6.

Adding RF power into beam heated plasmas would, in general, cause an increase of momentum diffusivity and affect the momentum pinch. Therefore, the observation of decreasing rotation with the addition of RF power can be due to either source or transport. To distinguish these two contributions would require a much cleverer experiment and comprehensive modeling. Based on the parametric dependence discussion in Section 3, we make a very simplified assumption that the rotation change is only due to a counter-I_p source in the core and neglect all the transport effect, and then estimate an effective torque. After the application of 1.8MW power at t = 11.35sec, the central rotation shown in Figure 8(a) decreases by approximately 3.5 krad/s. This change gives an instantaneous effect of approximately -2 krad/s per MW RF power, which is consistent with the -6 krad/s obtained when applying 3MW of RF power (Figure 6a). This estimate does not separate the rotation change due to the possible transport modification with the addition of RF power.

While an accurate estimate of the torque density profile would require detailed momentum transport modeling, we can have a very crude lowest order estimate of the torque density profile

using the break-in-slope of the rotation traces right before and after an RF transition (turn-on or turn-off),

This analysis is valid as long as the time window chosen is much shorter than the momentum confinement time. For these pulses, the total energy confinement time is about 0.4s, and the thermal energy confinement time is about 0.3s. The momentum confinement time is of this range or somewhat lower since Prandtl number $P_r \approx 1$ [22, 27]. At each RF transition, we calculate the breaks-in-slope as the average of the results from time windows of 30ms, 40 ms, and 50 ms before and after the transition (i.e., 3, 4 and 5 CXRS data points on both sides of the RF transition), and then we average the results of all 8 power transitions (4 turn-ons and 4 turn-offs) for $t > 11.35$sec, as labeled in Figure 8(a). The resultant torque density profile is shown in Figure 9, and the error bars are the standard deviations of the breaks-in-slope of different RF transitions. We assume the same rotation speed of bulk ions and the carbon impurity ions. To estimate the plasma mass, only D and ^{3}He ions are considered in the plasma neutrality equation and the electron density profile is from a High-Resolution Thomson scattering (HRTS) system. As shown in Figure 9, the counter-I_p torque profile peaks near-axis. For the outer-half ($R > 3.4$m), the torque density is much smaller but still in the counter–I_p direction. This small but negative effective torque density may explain the reduced co–I_p rotation in the outer-half of the MC plasmas in Figure 3 and 4. Although the torque density is largest near the plasma center, about a half of the integrated total torque comes from the outer-half of the plasma, $R \geq 3.4$m, due to a larger plasma volume. By volume integrating the torque density profile, the total counter-I_p torque is approximately -0.5Nm per MW RF power.

To give some perspective of the magnitude of this total torque, note that the angular momentum content of the directional ICRF fast waves at -90^o phase is about -0.1Nm per MW RF power, and a typical total torque expected from 1 MW neutral beam injection is ~ 1Nm on JET (cf. Fig.1(c) in Ref. [27]). The result from the above analysis indicates that the effective torque in the experiment could be as high as 50% of the neutral beam injection at the same power level and a factor of 5 larger than that carried by the launched fast waves.

5. FAST IONS DETECTION AND DEPENDENCE ON X[^{3}HE]

Direct fast particle losses can generate a counter-I_p torque and affect the plasma rotation [47]. In this section, we examine the fast ion losses in the plasmas from our experiment, and their dependence on X[^{3}He]. In this experiment, we did not have a neutral particle analyzer that was set up to measure ^{3}He so detailed spectra of ^{3}He ions are not available, but we can infer some of the qualitative information of the fast ion ^{3}He population from the data of a Scintillator Probe (SP) [44]. The SP allows the detection of lost ions at a single position outside the plasma, and provides the pitch angle and gyro-radius of the lost ions that are selected via a collimator. The light emitted by the scintillator is detected by a CCD camera and a PhotoMulTiplier (PMT) array. The lost ions include the fast particles generated by the ICRF heating - ^{3}He ions in these D(^{3}He) plasmas – and the proton and α-particles generated by nuclear reactions.

In Figure 10-(a), the CCD intensity vs. gyro-radius and pitch angle for Pulse No: 78848 integrated from t = 6 to 12sec are shown. The peak at a gyro-radius around 11cm corresponds to 3.6MeV α-particles generated from the nuclear reaction: $D^+ {}^3He \rightarrow {}^4He$ (3.6MeV) + p (14.7MeV). The proton is out of the detection range of the SP. The α-particle losses are prompt and proportional to the reaction rate. Using the measured pitch angle and gyro-radius, an orbit code can calculate the particle trajectories backward in time from the footprint, and infer the birth place of the α-particles. The hot region shown in Figure 10(a) corresponds to α-particles near the trapped and passing boundary born in the region between the ^{3}He ion cyclotron resonance (indicated by the red line) and the plasma center (at 56^o pitch-angle). The D and ^{3}He nuclear reaction cross-reaction is peaked between 200keV and 400keV, and decreases precipitously at lower temperature. The detection of these α-particles suggests that there is a hot ^{3}He ion population near the plasma center. In Figure 10(b) we plot the CCD intensity vs. the pitch angle at gyro-radius 11cm for different pulses at different X[^{3}He] levels. For Pulse No: 78825, where the ^{3}He level is low (X[^{3}He] < 0.5%), a very large peak (note 1/6 factor for this trace) appears around a pitch angle of 75 degrees, corresponding to passing α-particles born on the ^{3}He resonance layer and promptly lost (first orbit loss). The high intensity of the losses indicates that the 3He-ion tail in this pulse is rather energetic, and gamma-ray tomography [45] indicates a tail temperature of 200-250keV. Comparing the relative level and considering the reaction cross-section, we can qualitatively infer that to produce the level of α-particle losses observed in other pulses (X[^{3}He] ~ 13%) 78826, 78845 and 78848, a hot ^{3}He ion population (20-40keV) near the plasma center would be required. Note that a Maxwellian T_i at 4keV would not produce detectable α-particle loss in the SP data.

6. TORIC SIMULATION AND RF POWER DEPOSITION PROFILES

ICRF heating mechanism is very sensitive to the ^{3}He level in this D(^{3}He) plasmas as discussed in the Introduction. The strong dependence of the rotation profile and magnitude versus X[^{3}He] shown in Section 3 and fast ions dependence shown in Section 5 suggest that an X[^{3}He] dependent RF-mechanism may play an important role in flow drive. We have carried out a series of RF physics simulations using the 2-dimensional full wave ICRF code TORIC [48,49], which is a spectral code solving the wave field using toroidal and poloidal Fourier decompositions. This code calculates the RF power damping on species via the RF wave and particle interaction, and we run the code assuming Maxwellian ions and electrons. TORIC is a Finite Larmor Radius (FLR) code, and the MC ICW should be for most cases accurately modeled by the 2nd order FLR. The IBW branch has its damping rate modified consistently with the all orders electrostatic dispersion relation [50]. Collisional damping can be added and the wave equations can be solved together with transport equations, but here we only present the first order power partition among species. This is sufficient to show the most salient feature in RF physics versus X[^{3}He], which separates the minority heating regime, the intermediate MC regime, and the dominant MC regime. TORIC simulations can provide us with a 2-dimensional picture in power deposition and show the power partition among the wave

branches in detail. To simulate the flow drive experiment, we use an approximate JET plasma shape, analytic equilibrium fitted with experimental q_0 and I_p, and also experimentally measured T_e and n_e profiles. Each single TORIC run is carried out with a selected toroidal mode n_ϕ, and the maximum poloidal mode numbers m are set to be ±511, and 800 radial elements are used. This setup is adequate to have convergence for the mode conversion process. At -90^o phasing, the antenna spectrum for the JET A2 antennas peaks at the toroidal mode number, $n_\phi \approx k_\parallel R \approx -13$ [35, 40]. Without seeking more comprehensive modeling involving the antenna structure and plasma edge, we use this spectrum to approximate the one under the experimental conditions. To model properly the RF power deposition problem, we run simulations for each toroidal number individually, and convolve the contributions of the independent toroidal mode results with the antenna spectrum (similar to the method used in Ref. [12]). The result can qualitatively show the most important features of the RF physics.

In Figure 11-(a) and (b), we compare the power deposition from TORIC simulations at different X[^{3}He] (0.5%, 4%, 13% and 25%) and the experimentally obtained power deposition profiles. Experimentally, the direct RF power deposition to electrons can be estimated from the breaks-in-slope and Fourier analysis of the ECE Te signals [51]. An example of the breaks-in-slope in T_e traces can be seen in Figure 8-(c) at the RF transitions. In this part of this particular pulse, the electron response is dominated by sawteeth. As a result, the slopes (with and without RF) are strongly biased by the temperature redistribution due to the sawteeth, which has a similar timescale with the RF power modulation response itself, and this would make the resulted heating profile broader than the actual deposition profile. In this experiment, in pulses from 78845 to 78848 (X[^{3}He] ~ 12-14%) and pulse 78840 with X[^{3}He] ~ 25%, we have RF power modulations, thus break-in-slope and Fourier analysis can be carried out, and the result is show in Figure 11-(a). Profiles from experimental data are broader than those from the simulation due to the issues discussed above. The slight difference in the peak location for X[^{3}He] = 25% might be due to the uncertainty in X[^{3}He] measurement (A simulation using X[^{3}He] = 22% would show a better match). Since T_i (from CXRS) signals also subject to the sawteeth effect in addition to their poor temporal resolution, it is difficult to re-construct a reliable direct RF ion heating analysis from T_i signals. In Figure 11-(b), the ion deposition profile from experimental data obtained via Fourier analysis is compared to TORIC simulation, which shows a qualitative agreement. More experimental evidence on direct ion heating can be inferred from the fast ion measurement as discussed in Section 5.

ICRF mode conversion is a multi-dimensional process and geometry plays an important role. As a result, 2-dimensional contours of power deposition can provide a more detailed physics picture. In Figure 12 and Figure 13, we show such contours of RF power deposition to electrons and to ^{3}He ions respectively in five cases. Cases (a), (b), (c) and (d) are for 2.8 MA at different X[^{3}He], while case (e) is for 1.8MA and X[^{3}He] = 13%. All the contour plots have the same logarithmic scale in color, and the color of the lowest contour level is white and not shown. These contour plots show the trend of power partition versus X[^{3}He] via different waves and different mechanisms. In case (a), at X[^{3}He] = 0.5%, corresponding to Pulse No: 78825, almost all RF power is deposited on ^{3}He

ions via the fast wave (Figure 13(a)), while there is nearly no direct wave and electron interaction. Because the distance between the D-^{3}He hybrid layer and the ^{3}He IC layer is much shorter than the Doppler broadening of the IC resonance, there is no mode conversion. Note that the RF power to the small amount of ^{3}He ions generates a high energy ^{3}He ion tails (also indicated in Figure 10), and the tail slow-down will then transfer significant power to electrons via collisional damping (not modeled in this simulation). In case (b), at X[^{3}He] = 4%, corresponding to Pulse No: 78826, a small amount of direct electron heating is seen from the MC IBW on the High Field Side (HFS) of the MC layer, show in Figure 12(b), while most RF power is again deposited to ^{3}He ions via the fast wave near the ^{3}He cyclotron resonance as shown in Figure 13-(b). Case (c), at X[^{3}He] = 13%, corresponding to Pulse No: 78847, is the intermediate MC case. The electron heating is mostly via the MC ICW on the Low Field Side (LFS) of the MC layer, plus some from the MC IBW on the HFS of the MC layer, as shown in Figure 12-(c). Interestingly, ion heating from the MC ICW also becomes predominant near the plasma center as shown in Figure 13(c), although the FW ion cyclotron absorption of the ^{3}He ions (around R-R_0 = 0.20m) is still non-negligible. In case (d), at X[^{3}He] = 25%, corresponding to Pulse No: 78840, the electron heating is mostly via the mode converted ICW on the LFS of the MC layer (off-axis), as shown in Figure 12(d), and there is only small direct ion heating as shown in Figure 13(d). This is similar to the cases commonly used on JET as pure electron heating for electron transport studies. In case (e) at 1.8MA, the mode conversion picture is similar to case (c) that of 2.8MA, but noticeably, the branch of ICW below the mid-plane does not have ^{3}He interaction. Of these 5 cases, we observe the largest counter-I_p rotation in case (c) and case (e), and a smaller effect in case (d). In the next section, we propose a hypothesis to qualitatively account for the differences in torque generation in these cases.

7. UP-DOWN ASYMMETRY IN MODE CONVERSION PROCESS AND POTENTIAL ROLE IN TORQUE GENERATION

In order to generate plasma rotation, a net momentum input (like NBI) is not necessary. For example, in a plasma with a dipolar torque, there can be a net drive to plasma, and plasma rotation can be formed if the outer torque is transported to the edge faster than the inner one [52, 53]. Although the total canonical momentum (plasma + RF) is conserved, the MC ICW has larger momentum content than the fast wave by taking momentum from the plasma through non-resonant interactions. And the waves carry this additional momentum to where wave-particle resonance interactions occurs [54]. Moreover, the mode conversion to ICW is up-down asymmetric and thus a dipolar torque can be formed and potentially result in flow drive. In the following, we discuss this hypothesis in detail.

As shown in Refs. [11, 12, 13] from the analytic and numerical analysis of the MC ICW, simulation from TORIC and AORSA codes, and also experimental studies, the MC ICW solution only exists in a particular plasma region when the $|k_{||}|$ can be up-shifted to a large value so that a solution of the dispersion equation can be found. The $k_{||}$ up-shift is from the k transformation due to the field line transformation along the wave travelling path.

An approximation can be written as $k_{//} \approx \frac{1}{b_T}(b_p k_\theta + k_\phi) \sim \frac{m}{r}\frac{B_p}{B_t} + \frac{n_\phi}{R}$, with poloidal mode number m and toroidal number n_ϕ. For the ICW, the wave is propagating toward the LFS as shown in experiment [11], thus generally $m < 0$ above the mid-plane ($Z > 0$), and $m > 0$ for $Z < 0$. In the path of the wave, n_ϕ is conserved, while m is not conserved. To obtain the ICW at $Z > 0$, $k_\parallel$ needs to be significantly negative by acquiring a large negative m, while for the ICW at $Z > 0$, $k_\parallel$ needs to be significantly positive by a large positive m. To have a better idea of the momentum enhancement, we can estimate $k_\parallel$ from the TORIC simulation and plasma parameters. Using the ICW wavelength in the poloidal direction of about 5cm (from Figure 13(c)), we can estimate $m/r \sim -2\pi/\lambda \sim -125 m^{-1}$. At $r/a \sim 0.25$ and $q \sim 1$, we have $B_p/B_t \sim r/qR \sim 0.1$. With $n_\phi /R \sim -4.3 m^{-1}$, the ICW at $Z > 0$ has $k_{\parallel, ICW} \sim -17 m^{-1}$. Note this is a factor of 4 larger than the fast wave $k_\parallel$. FW $\sim n_\phi /R \sim -4.3 m^{-1}$. The same method gives $k_{\parallel, ICW} \sim 17 m^{-1}$ at $Z < 0$ with a different sign and at a different location ($r/a \sim 0.4$). Because Doppler broadening $\propto k_\parallel v_{ti}/\omega$, this significantly increased k|| also makes the ion cyclotron absorption of the ICW possible at the location farther away from the ^{3}He IC layer. In Figure 14, the power to the $Z > 0$ and $Z < 0$ branch of the MC ICW in the case of $X[^3He] = 13\%$ is integrated and plotted vs. r/a. Note the total RF power to ^{3}He shown in Figure 11(b) is the total power via MC ICW and fast wave. In this case, the portion of $Z > 0$ (thus, $k_\parallel < 0$) is significantly larger than the power from that of $Z < 0$. The parallel momentum carried by the waves is approximately proportional to $k_\parallel$. As a result, the process of mode conversion to ICW created two distinct zones in space: RF momentum in the counter–I_p direction for $Z > 0$ and co-I_p direction for $Z < 0$. This separation is determined by the direction of the plasma current, and is also affected by the launched fast wave direction (i.e., n_ϕ). The asymmetry shown in Figure 14 is the RF power deposition to ^{3}He ions, while the asymmetry in momentum would be much more complicated and its calculation is beyond the TORIC simulation.

For the case (e) in Figure 13(e) with I_p = 1.8MA, the mode conversion is different. The term $B_p/B_t \sim r/qR$ in the $k_\parallel$ transformation equation has a maximum vs. r/a, and it also depends on the plasma current profile. Generally, lower current makes the conversion to the ICW less favourable. In this particular case of 1.8MA, only the ICW above the mid-plane, that is, $m < 0$ and $k_\parallel < 0$, shows interaction with ^{3}He ions (Figure 13(e)). Below the mid-plane, the MC waves are mostly absorbed by electrons near the MC layer. As a result, although there is less total power converted to the MC ICW branch, the asymmetry in the ICW-ion interaction is still significant.

The mode conversion creates regions that are either counter–I_p or co–I_p wave dominated for the JET -90^o phase plasmas. Same as fast wave minority heating, the absorption mechanism of MC ICW ion heating is also ion cyclotron resonance interaction; therefore they have some similarities, for example, phase space diffusion and collisional balancing. However, it is different than fast wave minority heating in the sense that the ICW ion heating happens above and/or below the mid-plane with natural up-down asymmetry in real space and also in k space. The interaction between the MC ICW and the ^{3}He ions heats the ions to a much higher temperature than the background ions

as suggested from the fast ion loss SP measurement (Section 5). These hot ions carry the momentum from the waves. Because the heating is via the ion cyclotron resonance, the hot ions are more likely trapped due to a larger perpendicular velocity than parallel velocity. These trapped hot ions may transfer their momentum to the bulk ions via a return fast ion current or collision friction. For hot ions carrying momentum in the counter–I_p direction, their banana tips would move outwards, and a return inward radial current is generated to balance. This radial current then generates a bulk counter–I_p torque [55]. The detailed mechanism will be left for future work, for example, particle orbits modeling using the SELFO and ASCOT codes.

The RF interaction with the electrons should also impart the RF wave momentum to the plasma, but this interaction does not appear to help significantly drive rotation in our experiment and the result at X[^{3}He] = 25% shows less flow drive. There are two possible reasons. First, cross field radial current is a key, and this can only arise from ion interactions because electrons are bound on the field lines. Second, electron absorption does not have as large asymmetry as that for ^{3}He ions absorption as discussed above. The MC IBW heats the electrons near the mid-plane and no k|| up-shift. For the MC ICW, the electron absorption occurs in the vicinity of the MC layer, i.e., as soon as the mode conversion happens, where the $k_{||}$ of the wave is not much different than the fast wave, and the power deposition zones above and below the mid-plane tend to cancel each other, leaving little asymmetry in the flux surface average. This may explain the lower flow drive efficiency at high ^{3}He ratio (e.g. 25% ^{3}He), where the MC layer is too far away for any cyclotron resonance absorption of the ICW. In the minority heating scenario, the fast wave heating practically does not have up-down asymmetry (Figure 13(a)), and no momentum enhancement is expected. In an experiment reported previously [36], the momentum input by the fast wave launched at -90^o was found to be not insignificant, but could only explain a part of the observed rotation in minority heating experiment.

In summary, the mode conversion process may result in momentum asymmetry and generate a net torque. This mechanism may be an important (although not exclusive) contributor for the experimentally observed flow drive effect. More detailed experimental study and theoretical development are needed to test the hypothesis.

8. DISCUSSION

RF waves act as a momentum source and energy source, generate fast particles, affect transport by heating electrons and ions, and also modify turbulence. A pure transport argument cannot explain all of our experimental results. The plasmas remain in L-mode and a sudden change near the edge is less likely although it is not completely ruled out due to possible RF edge interactions. Sole momentum from the plasma edge transport, i.e., momentum diffusion, re-distribution and pinch, would not create a counter–I_p rotation in the core with the edge rotating in the co–I_p direction. The reversal of rotation from co–I_p to counter–I_p is a clear indicator of a counter–I_p torque source in the core.

In the JET experiment reported in this paper, we scanned the X[^{3}He] level from the minority heating, intermediate MC regime, and dominant MC electron heating region. The rotation behavior

in the minority heating regime in our experiment is similar to that found in previous JET ICRF rotation studies [34], but the behavior in the intermediate X[^{3}He] regime is definitely different than either the minority heating regime, or the dominant MC electron heating regime. We have also established a P_{RF} dependence of this effect. The dependences on PRF and X[^{3}He] are similar to those observed in the experiments on Alcator C-Mod, suggesting that both experiments may have similar RF physics origin. In Section 7, we qualitatively proposed a hypothesis that the up-down asymmetry in the mode conversion process to the MC ICW may contribute the counter-I_p torque observed in the JET plasmas at -90^o phasing. Unfortunately, in this experiment, we did not have data in other antenna phasings. As shown in another JET mode conversion experiment in (H)–D–^{3}He plasmas with dipole phase (the net direct toroidal momentum is close to zero), enhanced rotation in the counter-I_p direction has also been observed [56]. With dipole phasing, there is approximately equal power in -90^o ($n_\phi > 0$) and $+90^o$ phasing ($n_\phi > 0$) in the launched FW power. With $+90^o$ phasing ($n_\phi > 0$) the up-down asymmetry would still exist, but because the direction of Ip plays an important role in mode conversion, it is not a mirror image of -90^o phasing. Therefore, even for dipole phasing, after mode conversion the RF momentum from positive and negative toroidal mode numbers do not cancel out in space and a dipolar torque can be generated. However, the magnitude or the direction of the net torque cannot be easily assessed. In similar D(^{3}He) experiments on Alcator C-Mod, the rotation has been to shown to increase toward the co-I_p direction compared to the ICRF minority heating. The effect has a very similar dependence on X[^{3}He]. The rotation increase at -90^o phasing is generally smaller than that at dipole and $+90^o$ phasing, and possibly a counter-I_p torque exists at the high RF power level [37, 38]. As a result, the experimental results from Alcator C-Mod and JET give a very complicated picture and they do not fully agree to each other. Alcator C-Mod is a much smaller tokamak than JET, and most wave parameters are not scalable vs. the machine size. Many other issues can be in play, for example, the mode conversion efficiency at different n_ϕ, MC location and different hot ions orbits. The up-down asymmetry must also play an important role in the Alcator C-Mod experiment, but there may well be other more complicated mechanisms (for example, associated transport) that contributes. To reconcile the apparent discrepancies, we will need more experiments on these two tokamaks plus theoretical research in order to explain the direction and magnitude of the rotation and its dependence on other plasma parameters.

In NBI heated plasmas with toroidal rotation, it is common that application of ICRF power tends to slow down the plasma rotation due to the modification of turbulence and momentum transport with RF heating [57, 58]. Lost fast trapped ions (an ion is traveling in the co-current direction on the outer leg of its orbit, and a loss of it will therefore give a counter-current torque on the plasma) can also provide a counter–I_p torque. Counter–I_p rotation by ICRF alone was observed in TFTR minority heating plasmas due to the loss of fast ions [47]. On TORE SUPRA counter-Ip rotation was observed at low minority concentration with ripple induced fast ion loss [32], while on JET, counter-I_p rotation in ICRF heated plasmas can be generated by fast ion losses, either enhanced by deliberately introduced toroidal field ripple [59, 60] or high RF power [61]. In our experiment, the

toroidal field ripple is the usual level (~ 0.08%), and in the mode conversion pulses, fast ion losses should not be a main contribution to the counter-Ip torque, as discussed in Section 5. Otherwise, Pulse No: 78825, having much more significant fast ion losses, would have a larger counter–I_p rotation than other pulse, but it is not the case experimentally.

MHD modes, sawteeth, and Toroidal Alfven Eigenmode (TAE) activities may also create counter-I_p rotation. Rotation in high I_p ICRF minority heated plasmas on JET is generally co–I_p, but in large sawtooth regimes, especially when core TAE modes are present, counter–I_p rotation in the core has been observed [59]. This possibility can be ruled out for our L-mode plasmas with modest heating power.

Recently, in some JET pulses heated with 2nd harmonic ^{3}He fast waves, counter–I_p rotation has also been observed [56]. In these plasmas, no ICRF mode conversion is involved, but possibly a different mechanism is contributing to the observed change in rotation.

Dedicated future experiments in different plasma confinement modes, antenna phasing and higher RF power will help further understand this flow drive mechanism, and help resolve the intriguing difference with the results from Alcator C-Mod. If we can find a way that ICRF mode conversion can substantially drive rotation under certain plasma conditions on JET, this flow drive method can have a much broader and more interesting applicability in existing tokamaks and future devices such as ITER.

SUMMARY

ICRF mode conversion has been shown to drive toroidal flow in JET D(^{3}He) L-mode plasmas. At X[^{3}He] = n_{He3}/ne ~ 10–17%, peaked rotation in the counter-I_p direction has been observed, in contrast to the slow co–I_p rotation observed in ICRF minority heated plasmas. The central rotation in these mode conversion plasmas scales with the input RF power, and velocities $\omega_{\phi 0}$ up to 10krad/s (~30km/s) have been observed. The total torque from the process is estimated to be up to 50% of the same power from neutral beam injection, and a factor of approximately 5 higher than that from the fast wave direct momentum input. RF physics modeling using the TORIC code has been carried out and the MC wave power deposition on ions and the spatial and momentum asymmetry associated with this process may be the key to explain the torque. Further experiments on JET and other tokamaks and theoretical research will help shed light on the detailed flow drive physics in order to understand and control the sign of MC flow drive and to optimize the flow drive efficiency.

ACKNOWLEDGEMENTS

This work is supported by IEA Implementing Agreement on co-operation on the Large Tokamak Facilities between Alcator C-Mod and JET. Alcator C-Mod is supported by US DoE Cooperation Agreement DE-FC02-99ER54512 at MIT. Computer simulations using TORIC were carried out on the MIT PSFC parallel AMD Opteron/Infiniband cluster Loki. This work was supported by EURATOM and carried out within the framework of the European Fusion Development Agreement. The views and opinions expressed herein do not necessarily reflect those of the European Commission.

REFERENCES

[1]. Burrell K.H. 1997 Physics of Plasmas **4** 1499

[2]. Mantica P. et al 2009 Physical Review Letters **102** 175002

[3]. Politzer P.A. et al 2008 Nuclear Fusion **48** 075001

[4]. Strait E.J. et al 1995 Physical Review Letters **74** 2483

[5]. Garofalo A.M. et al 2001 Nuclear Fusion **41** 1171

[6]. Lin Y. et al 2008 Physical Review Letters **101** 235002

[7]. Lin Y. et al 2009 Physics of Plasmas **16** 056102

[8]. Porkolab M. 1994 Plasma heating by fast magnetosonic waves in tokamaks, N. Fisch ed. Advances in Plasma Physics, AIP Conference Proceedings. Vol **304** p99

[9]. Perkins F.W. 1977 Nuclear Fusion **17** 1197

[10]. Adams J. 1987 Plasma Physics and Controlled Fusion **29** 443

[11]. Nelson-Melby E. et al 2003 Physical Review Letters **90** 155004

[12]. Lin Y. et al 2005 Plasma Physics and Controlled Fusion **47** 1207

[13]. Jaeger E.F. et al 2003 Physical Review Letters **90** 195001

[14]. Mantsinen M.J. et al 2004 Nuclear Fusion **44** 33

[15]. Van Eester D. et al 2009 Plasma Physics and Controlled Fusion **51** 044007

[16]. Mantica P. et al 2006 Physical Review Letters **96** 095002

[17]. Mayoral M.-L. et al 2006 Nuclear Fusion **46** S550

[18]. Parisot A. et al 2007 Plasma Physics and Controlled Fusion **49** 219

[19]. deGrassie J.S. et al 2009 Plasma Physics and Controlled Fusion **51** 124047

[20]. Rice J.E. et al 2007 Nuclear Fusion **47** 1618

[21]. Solomon W. et al 2010 Physics of Plasmas **17** 056108

[22]. Tala T. et al 2009 Physical Review Letters **102** 075001

[23]. Rice J. et al 2009 Nuclear Fusion **49** 025004

[24]. Yoshida M. et al 2009 Physical Review Letters **103** 065003

[25]. Nave M.F.F. et al 2010 Physical Review Letters **105** 105005

[26]. Bortolon A. et al 2006 Physical Review Letters. **97** 235003

[27]. de Vries P.C. et al 2008 Nuclear Fusion **48** 065006

[28]. Rice J.E. et al 1999 Nuclear Fusion **39** 1175

[29]. Hutchinson I.H. et al 2000 Physical Review Letters **84** 3330

[30]. Eriksson L.-G., et al 1997 Plasma Physics and Controlled Fusion **39** 27

[31]. Assas S. et al 30th EPS Conf. on Plasma Physics and Controlled Fusion (St Petersburg, Russia, 7-11 July 2003) ECA 27A, P-1.138.

[32]. Eriksson L.-G. et al 2001 Nuclear Fusion **41** 91.

[33]. Assas S. et al 2007 Radio Frequency Power in Plasmas, edited by P.M. Ryan and D. A. Rasmussen, AIP Conference Proceedings **978** 103.

[34]. Eriksson L.G. et al 2009 Plasma Physics and Controlled Fusion **51** 044008

[35]. Noterdaeme J.-M. et al 2003 Nuclear. Fusion **43** 274
[36]. Eriksson L.-G. et al 2004 Physical Review Letters **92** 235001
[37]. Rice J. et al 37th EPS conference on Plasma Physics (Dublin, Ireland, 21-25 June, 2010)
[38]. Lin Y. et al 23rd IAEA Fusion Energy Conference (Daejeon Korea, 11-16 October 2010), EXW/4-1, to be submitted to Nuclear Fusion.
[39]. Noterdaeme J.-M. et al 2008 Fusion Science and Technology **53** 1103
[40]. Kaye A. et al 1994 Fusion Engineering Design **24** 1
[41]. Negus C.R. et al 2006 Review of Scientific Instruments **77** 10F102
[42]. Giroud C. et al 2008 Review of Scientific Instruments **79** 10F525
[43]. Baeumel S. et al 2004 Review of Scientific Instruments **75** 3563
[44]. Kiptily V. et al 2009 Nuclear Fusion **49** 065030
[45]. Kiptily V. et al 2009 Plasma Physics and Controlled Fusion **48** R59
[46]. de la Luna E. et al 2004 Review of Scientific Instruments **75** 3831
[47]. Hsuan H. et al 1995 11th Topical Conf. on RF Power in Plasmas (Palm Springs, 1995) AIP Conference Proceedings Vol 355 p39
[48]. Brambilla M. 1999 Plasma Physics and Controlled Fusion **41** 1
[49]. Wright J. C. et al 2004 Physics of Plasmas **11** 2473
[50]. Brambilla et al 1988 Nuclear Fusion **28** 1813
[51]. Lerche E. et al 2008 Plasma Physics and Controlled Fusion **50** 035003
[52]. Perkins F.W. et al 2001 Physics of Plasmas **8** 2181
[53]. Myra J.R. et al 2002 Physics of Plasmas **9** 3867
[54]. Hellsten T. 2009 16th Topical Conf. on RF Power in Plasmas (Gent, Belgium, 2009) AIP Conference Proceedings Vol 1187 P625
[55]. Hinton F.L. et al 1999 Physics of Letters A **259** 267
[56]. Hellsten T. et al 2010 submitted to Plasma Physics and Controlled Fusion (this issue).
[57]. Nishijima D. et al 2005 Plasma Physics and Controlled Fusion **47** 89
[58]. de Grassie J.S. et al 16th Topical Conf. on RF Power in Plasmas (Park City, 2005) AIP Conference Proceedings Vol 787 p110
[59]. Nave M.F.F. et al 37th EPS conference on Plasma Physics (Dublin, Ireland, 21-25 June, 2010)
[60]. de Vries P.C. et al 2008 Nuclear Fusion **48** 035007
[61]. Hellsten T. et al 1999 Nuclear Fusion **44** 892

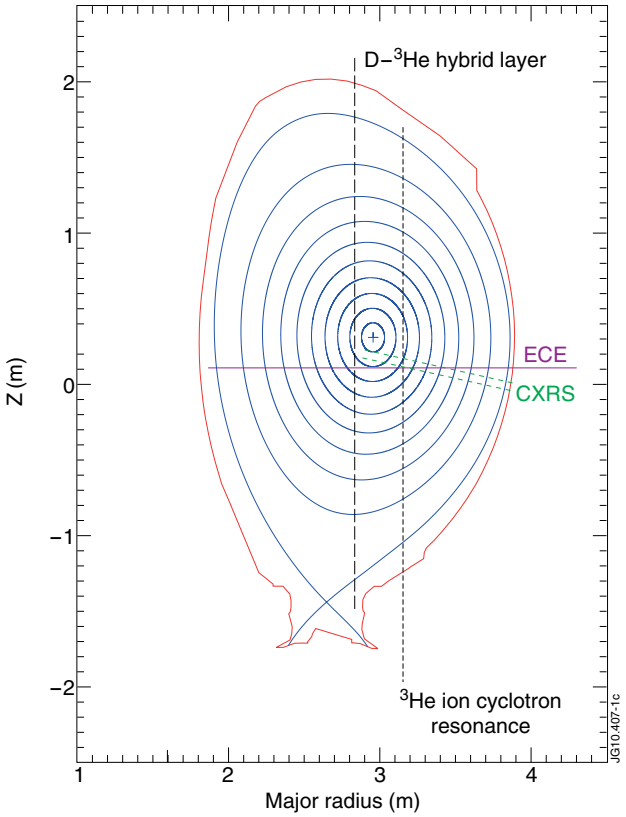

Figure 1: Plasma configuration for the experiment (R_0 ≈ 2.96m). The ^{3}He cyclotron resonance layer and mode conversion layer for X[^{3}He] = 13% are labeled. The interactions of CXRS periscopes and the viewing line of the ECE diagnostic are also shown.

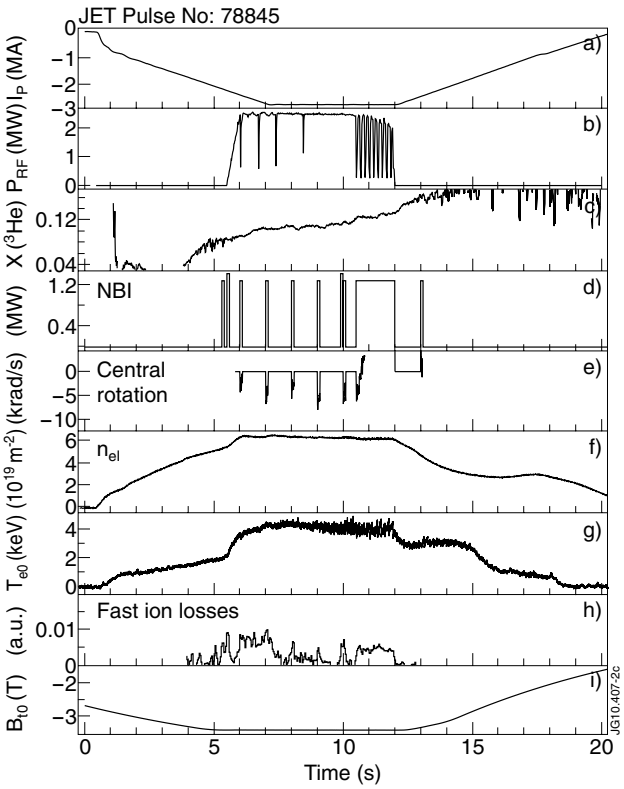

Figure 2: Data traces from Pulse No: 78845: (a) I_p; (b) PRF ; (c) X[^{3}He]; (d) Neutral beam power; (e) Rotation at R = 3.04 m; negative value indicates counter-I_p rotation; (f) Line integrated density, corresponding to central density n_{e0}~ 3×10^{19} m^{-3} during flat top; (g) Central T_e; (h) fast α-particle loss signal from a scintillator probe; (i) Toroidal B field.

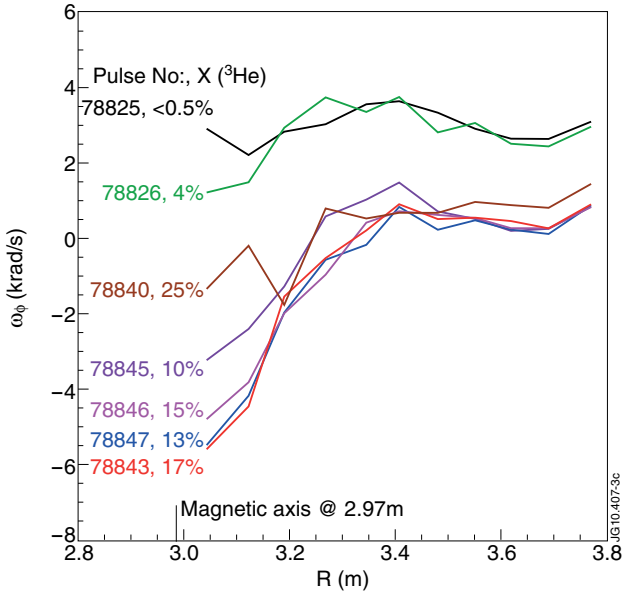

Figure 3: Toroidal rotation profiles from 2.8MA pulses at different X[^{3}He] (PRF 1.8 to 3MW). Data are taken at t = 7sec (except that Pulse No: 78840, at t = 6.5 sec). Negative ω_ϕ is defined as in the counter-Ip direction. The magnetic axis is at R_0 = 2.97m and separatrix R_{sep} is approximately 3.90m.

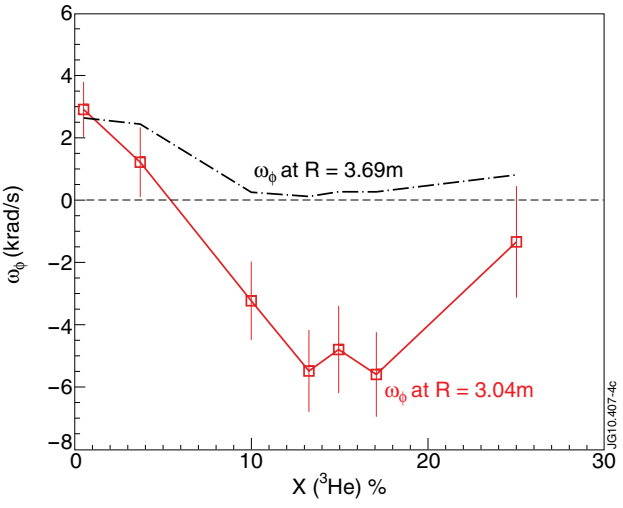

Figure 4: Rotation at R = 3.04m and R = 3.69m versus X[^{3}He] (same data as those in Figure 3).

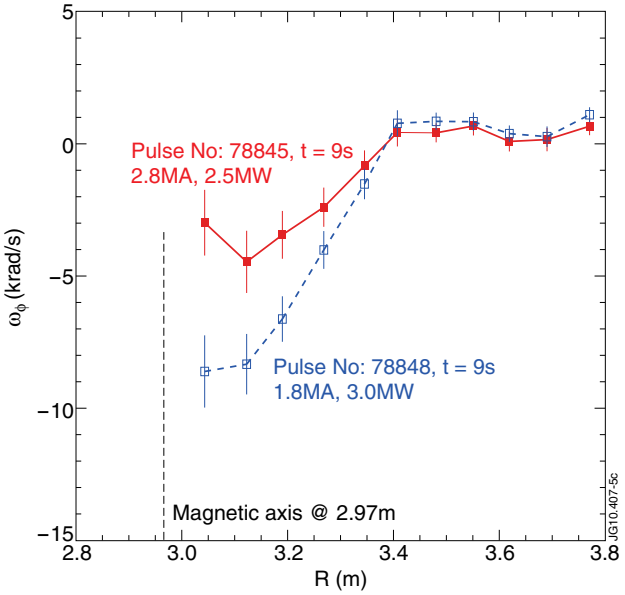

Figure 5: (Color online) Rotation profiles at 2.8MA and 1.8MA. X[3He] = 12%-13% for both pulses. The magnetic axis is at R_0 = 2.97m and separatrix Rsep is approximately 3.90m.

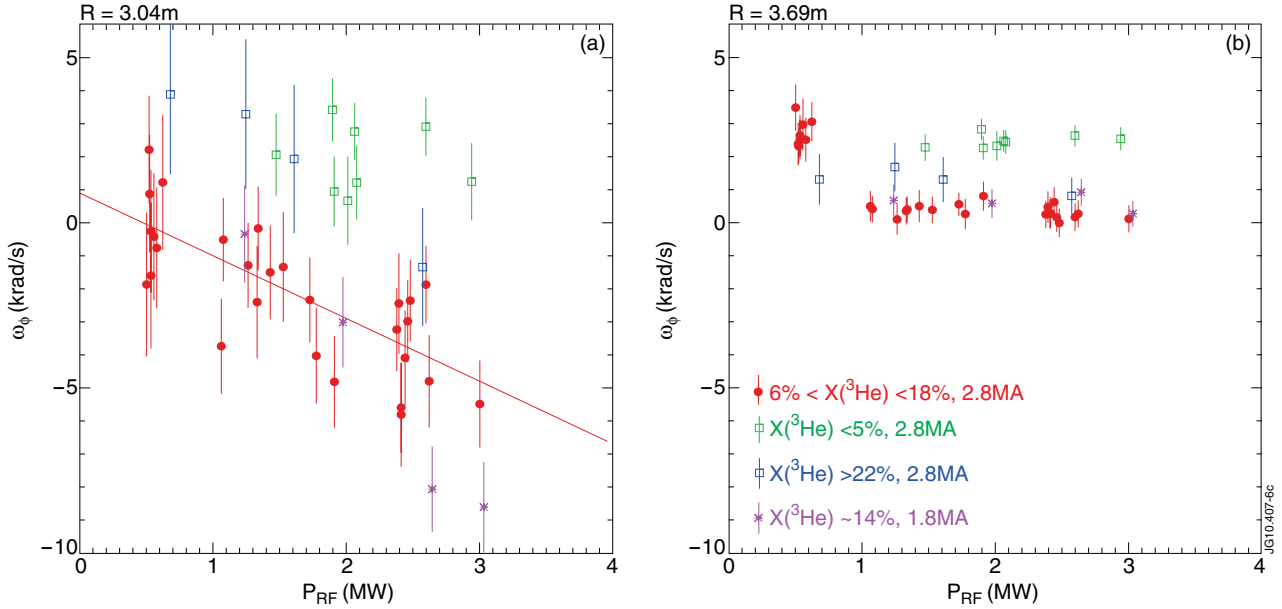

Figure 6: (Color online) Rotation at (a) R = 3.04m and (b) R = 3.69m vs. input RF power. A linear fit is also indicated for the data of 6% < X[^{3}He] <18%. Negative ω_ϕ is defined as in the counter-I_p direction.

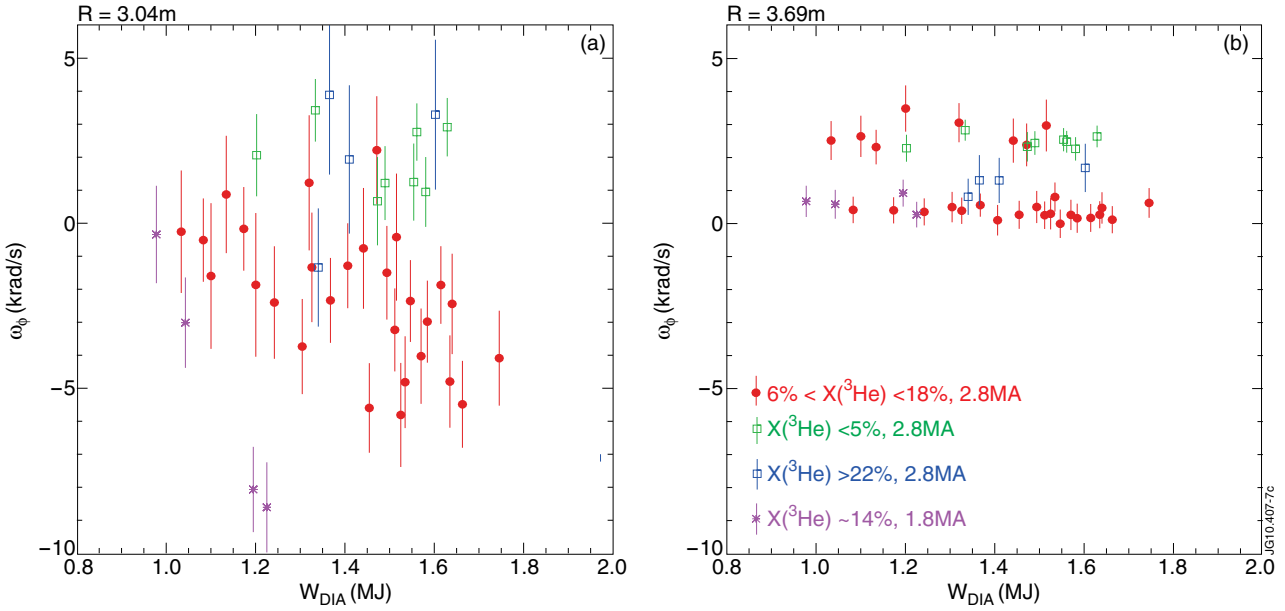

Figure 7: Rotation at (a) R = 3.04m and (b) R = 3.69m versus plasma stored energy W_{dia}.

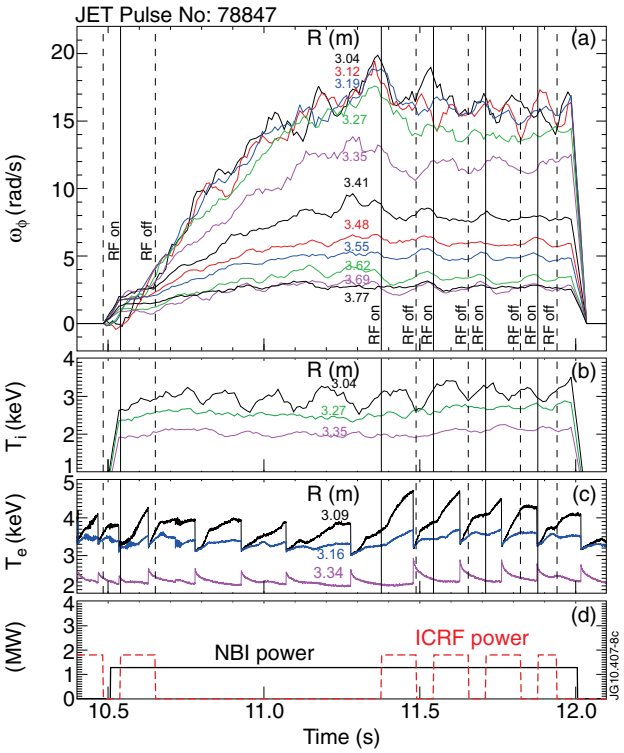

Figure 8: Rotation and T_e responses vs. RF modulation: (a) Rotation time traces at different major radii with RF on and RF off labelled; (b) Ti time traces; (c) T_e time traces; (d) NBI power and RF power.

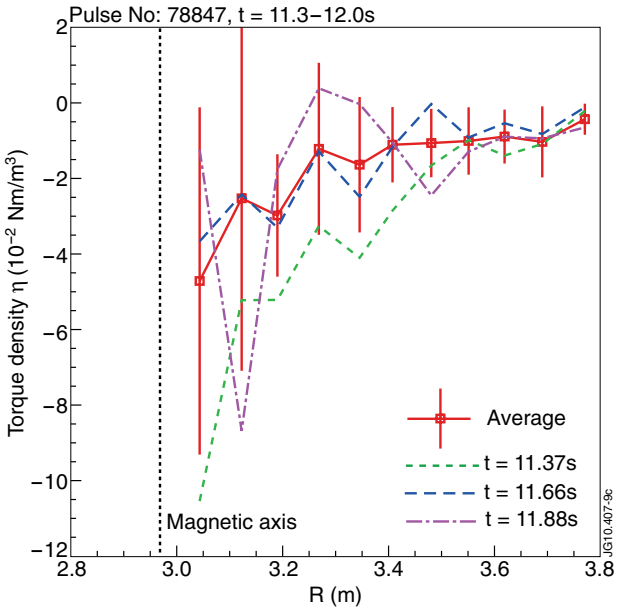

Figure 9: Estimated torque density profile resulted from 1.8MW RF power (X[^{3}He] = 13%, Pulse No: 78847). The red solid curve is the average of all eight RF power transitions shown in Figure 8. Results of three selected RF power transitions are also plotted. $R_{sep} \approx 3.90$m and magnetic axis $R_0 \approx 2.97$m.

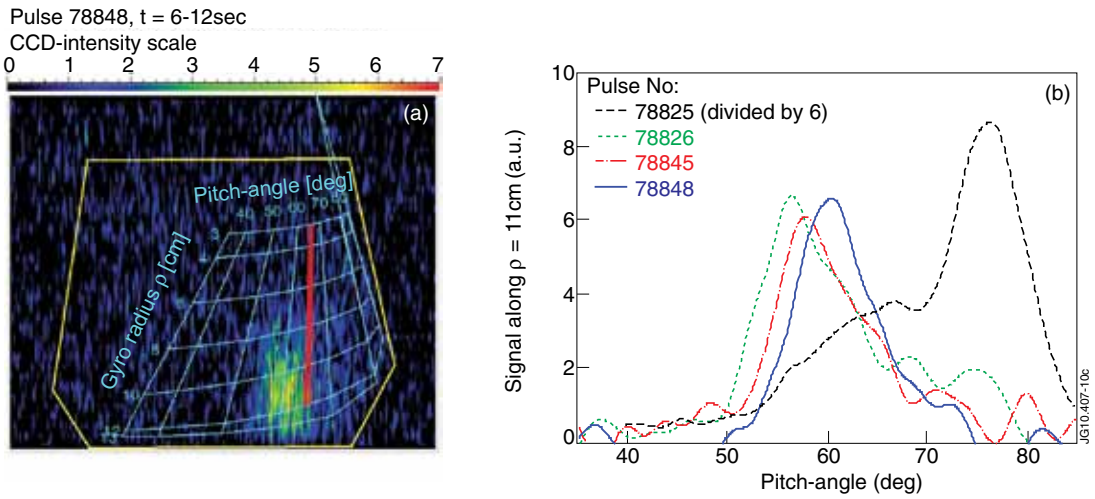

Figure 10: (a) Fast ion loss in gyro-radius and pitch angle from SP for Pulse No: 78848; Red line indicate particles born from the mid-plane of the IC resonance; (b) fast ion loss profile at gyro-radius of 11cm (~3.6MeV α-particles) versus pitch-angle for different pulses.

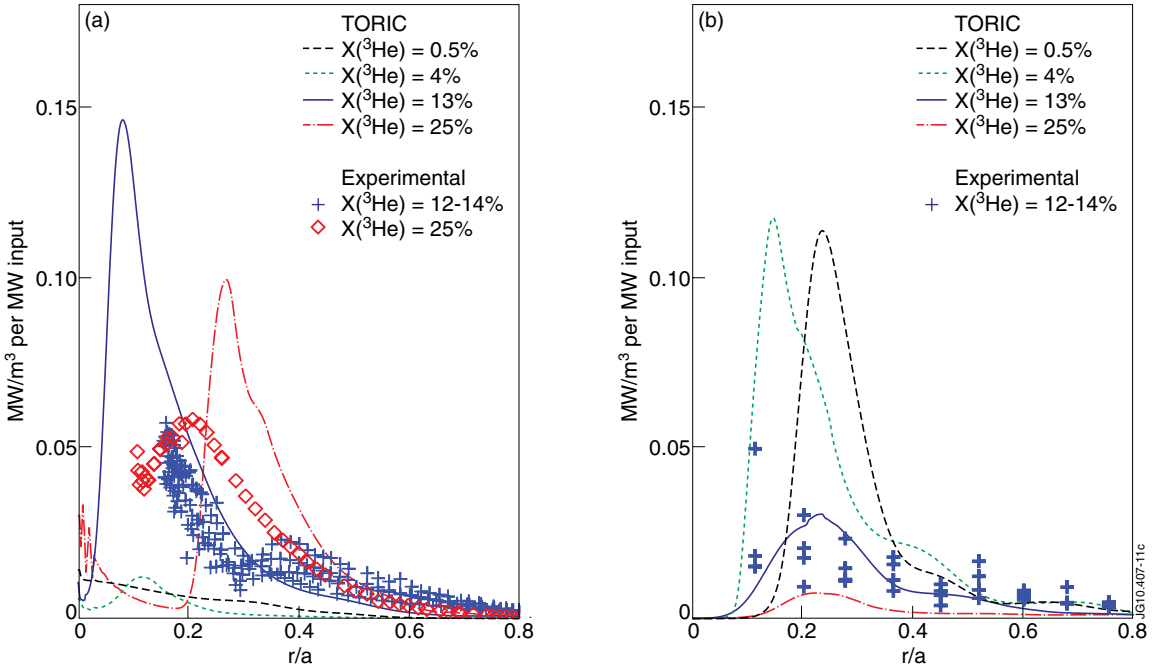

Figure 11: Power deposition profiles from TORIC simulation for X[^{3}He] = 0.5%, 4%, 13% and 25% and also from experimental measurement for X[^{3}He] =12-14% and 25%. (a) Power to electrons, (b) Power to ^{3}He ions.

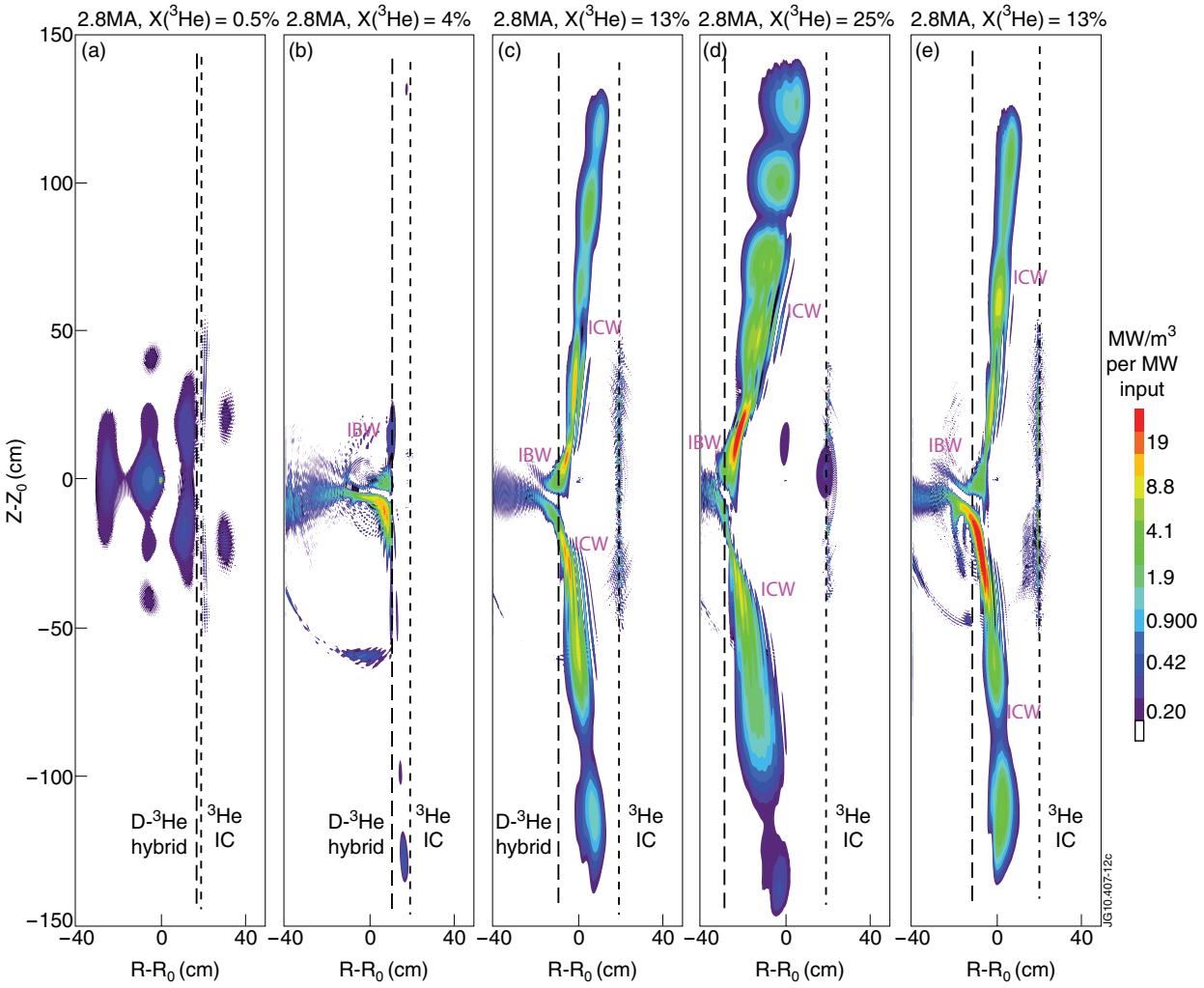

Figure 12: 2D power deposition to electrons from TORIC simulations (toroidal mode = -13): a) 2.8MA, X[^{3}He] = 0.5%; (b) 2.8MA, X[^{3}He] = 4%; (c) 2.8MA, X[^{3}He] = 13%; (d) 2.8MA, X[^{3}He] = 25%, (e)) 1.8MA, X[^{3}He] = 13%; MC wave branches are labelled. R_{sep} = 3.90m, and R_0 = 2.97m.

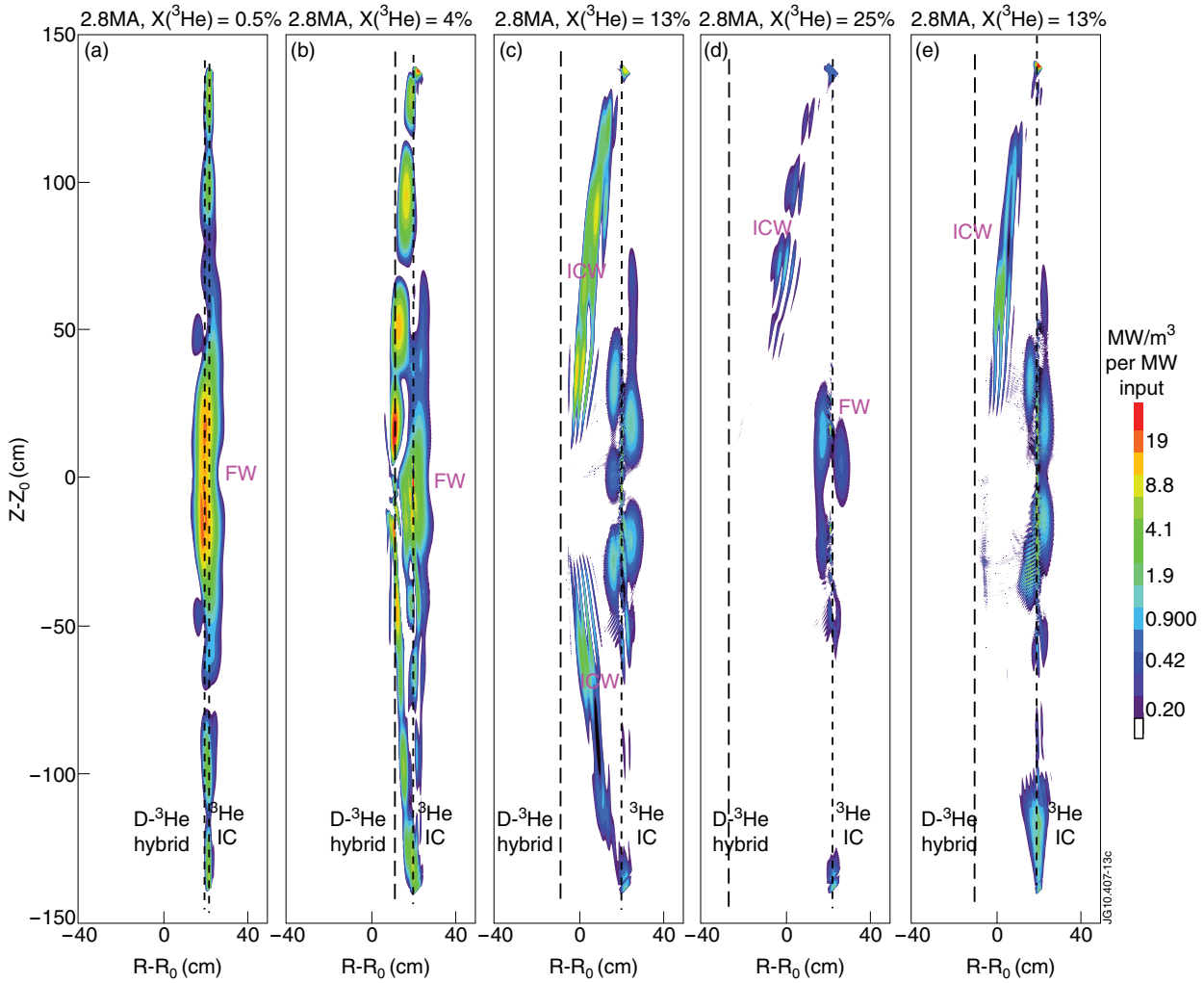

Figure 13: (Color online) 2D power deposition to ^{3}He ions from TORIC simulations (toroidal mode = −13): a) 2.8MA, X[^{3}He] = 0.5%; (b) 2.8MA, X[^{3}He] = 4%; (c) 2.8MA, X[^{3}He] = 13%; (d) 2.8MA, X[^{3}He] = 25%, (e)) 1.8MA, X[^{3}He] = 13%; MC wave branches are labelled. R_{sep} = 3.90m, and R_0 = 2.97m.

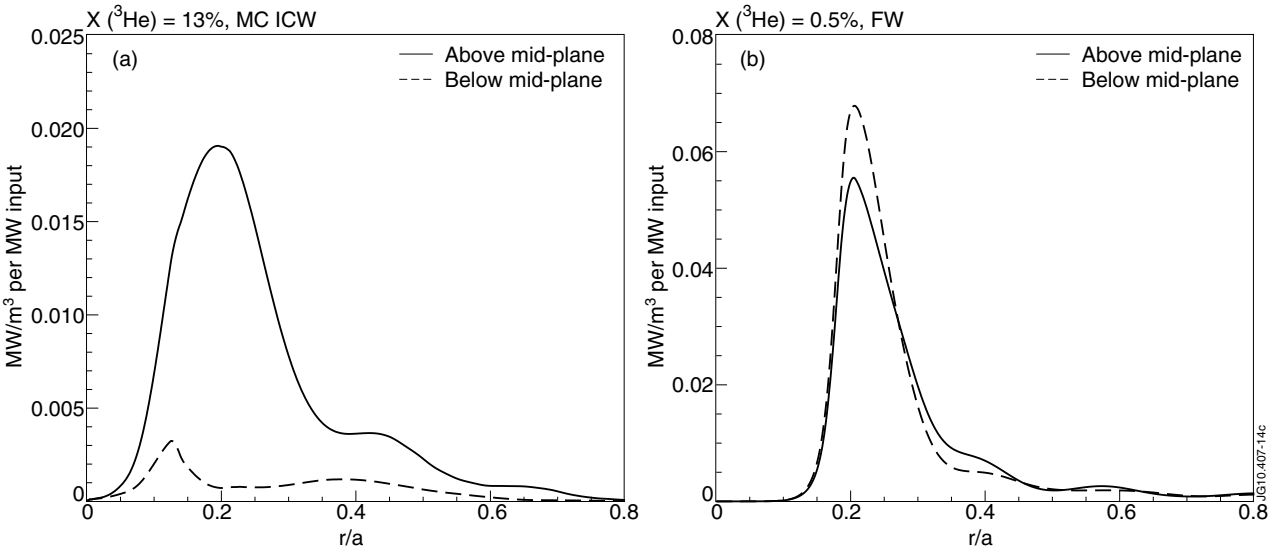

Figure 14: (a) Up-down asymmetry in RF power deposition to 3He ions via the MC ICW for X [^{3}He] = 13% and I_p = 2.8MA; (b) RF power deposition to 3He ions via the fast wave for X [^{3}He] = 0.5% an I_p = 2.8MA